J Biol Inorg Chem
DOI 10.1007/s00775-015-1292-0

ORIGINAL PAPER

Investigation of the salicylaldehyde thiosemicarbazone scaffold for inhibition of influenza virus PA endonuclease

Dominga Rogolino[1] · Alessia Bacchi[1] · Laura De Luca[2] · Gabriele Rispoli[1] · Mario Sechi[3] · Annelies Stevaert[4] · Lieve Naesens[4] · Mauro Carcelli[1]

Received: 18 February 2015 / Accepted: 4 August 2015

Abstract The influenza virus PA endonuclease is an attractive target for the development of novel anti-influenza virus therapeutics, which are urgently needed because of the emergence of drug-resistant viral strains. Reported PA inhibitors are assumed to chelate the divalent metal ion(s) (Mg^{2+} or Mn^{2+}) in the enzyme's catalytic site, which is located in the N-terminal part of PA (PA-Nter). In the present work, a series of salicylaldehyde thiosemicarbazone derivatives have been synthesized and evaluated for their ability to inhibit the PA-Nter catalytic activity. Compounds **1**–**6** have been evaluated against influenza virus, both in enzymatic assays with influenza virus PA-Nter and in virus yield assays in MDCK cells. In order to establish a structure–activity relationship, the hydrazone analogue of the most active thiosemicarbazone has also been evaluated. Since chelation may represent a mode of action of such class of molecules, we studied the interaction of two of them, one with and one without biological activity versus the PA enzyme, towards Mg^{2+}, the ion that is probably involved in the endonuclease activity of the heterotrimeric influenza polymerase complex. The crystal structure of the magnesium complex of the *o*-vanillin thiosemicarbazone ligand **1** is also described. Moreover, docking studies of PA endonuclease with compounds **1** and **2** were performed, to further analyse the possible mechanism of action of this class of inhibitors.

Keywords Influenza virus · Thiosemicarbazone · Endonuclease · Metal chelation · Antiviral

Introduction

Currently available antiviral drugs to treat or prevent influenza infections comprise two classes of agents: those targeting the viral M2 ion-channel (amantadine and rimantadine) and those targeting the viral neuraminidase (NA) (zanamivir and oseltamivir). The M2 inhibitors have limited clinical utility because of worldwide spread of drug-resistant mutant viruses among almost all influenza A virus subtypes, including the 2009 pandemic H1N1 virus [1–3]. Resistance is also a growing concern for oseltamivir [4]. Therefore, there is an urgent need for entirely novel antiviral compounds with a different mode of action and targeting a critical step in the viral replication process [5]. The influenza virus genome consists of eight single-stranded (−)RNA segments, which are transcribed and replicated by the viral RNA-dependent RNA polymerase (RdRp) [6, 7]. This RdRp is widely recognized as a superior target for the development of new antivirals, since it is highly conserved among influenza A, B and C viruses, and its functions are essential for viral genome replication [8]. It is composed of three subunits: PA, PB1 and PB2. The endonuclease activity, which resides in the N-terminal part of PA (PA-Nter) [9,

Electronic supplementary material The online version of this article (doi:10.1007/s00775-015-1292-0) contains supplementary material, which is available to authorized users.

✉ Mauro Carcelli
mauro.carcelli@unipr.it

[1] Dipartimento di Chimica, Università di Parma, Parco Area delle Scienze 17/A, 43124 Parma, Italy

[2] Dipartimento di Scienze del Farmaco e Prodotti per la Salute, Università di Messina, Polo Universitario SS. Annunziata, 98158 Messina, Italy

[3] Dipartimento di Chimica e Farmacia, Università di Sassari, Via Vienna 2, 07100 Sassari, Italy

[4] Rega Institute for Medical Research, KU Leuven, 3000 Louvain, Belgium

Published online: 01 September 2015

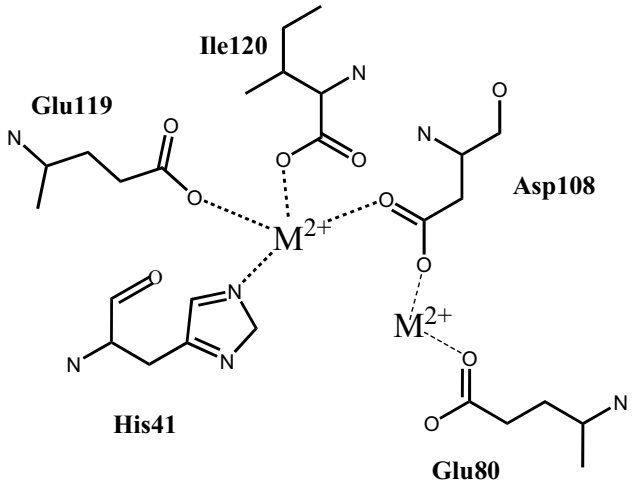

Fig. 1 Schematic representation of the metal-interacting residues within the catalytic site of influenza virus PA endonuclease, assuming the presence of two metal ions (see Ref. [12, 13])

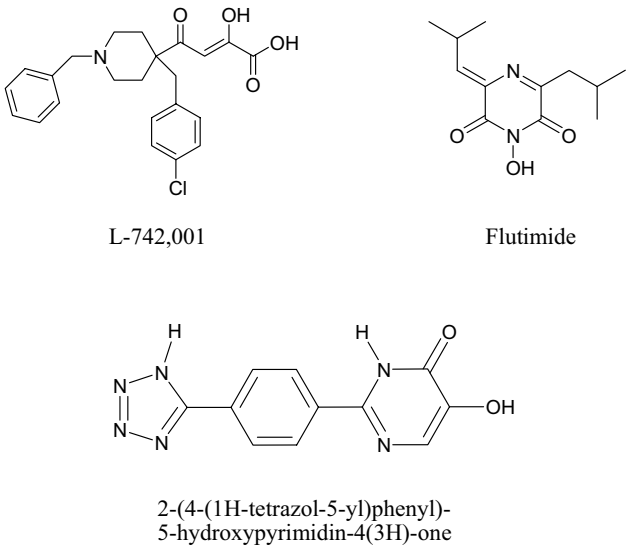

Fig. 2 Chemical structures of some prototype inhibitors of influenza virus endonuclease [19, 21, 24]

10], is required to cleave host cell pre-mRNAs and produce the 5′-capped primers for transcription of the viral genomic RNA into mRNA (cap-snatching) [11]. Cap-snatching is an important event in the life cycle of all members of the *Orthomyxoviridae* family of viruses, including influenza A, B and C viruses. The host cell has no analogous activity; therefore, inhibitors of cap-snatching may be active against all influenza virus (sub)types and strains, including oseltamivir-resistant influenza viruses, without interfering with normal host cell functions.

Several X-ray crystallographic studies have been performed on PA-Nter, revealing the presence of one [10, 12] or two [9, 13, 14] divalent metal ions within the active site (Fig. 1). The two-metal-ion model is also consistent with biochemical [15] and computational [16] findings. The ions identified by means of X-ray diffraction are magnesium(II) or manganese(II), depending on the crystallization conditions. Considering the relative abundance of these two metal ions in the cell ($[Mg^{2+}]$ is about 1000 times higher than $[Mn^{2+}]$), magnesium may be more biologically relevant.

Metal chelation has emerged as an efficient strategy to develop new inhibitors of metal-dependent viral enzymes, the most illustrious example being the class of HIV integrase inhibitors, some of which have already been approved [17]. In the same way, development of PA-binding agents with metal-chelating properties may represent a successful strategy to tackle influenza infections. Several chelating molecules have been identified as influenza endonuclease inhibitors, including 2,4-dioxobutanoic acid derivatives [18–20], 5-hydroxy-1,6-dihydropyrimidine-4-carboxylic acids [12], flutimide and its derivatives [21], 2-hydroxyphenyl amide derivatives [22] as well as tetramic acids [23] and 5-hydroxy pyrimidin-4-one derivatives [24] (Fig. 2).

Thiosemicarbazones (TSCs) possess a broad range of biological properties including antitumor, antimalarial and antimicrobial activity [25]; moreover, they have shown good antiviral activity against herpes simplex virus [26], vaccinia and cowpox virus [27], as well as HIV [28, 29]. The biological properties of TSCs are often related to chelation of metal ions [30] and, therefore, they could be good candidates as chelating inhibitors of influenza virus endonuclease. TSCs can coordinate to the metal centre in an *N*,*S*-bidentate mode, but when an additional coordinating group is present, more diversified binding modes become possible [31]. In particular, the presence of the OH group in salicylaldehyde thiosemicarbazone derivatives might provide a more favourable coordination for hard metal ions like Mg^{2+} that prefers oxygen donor atoms.

In the present work, we report the synthesis of some salicylaldehyde thiosemicarbazone derivatives (**1**–**6**, Fig. 3) and their biological evaluation against influenza virus, both in enzymatic assays with influenza virus PA-Nter and in virus yield assays in MDCK cells. In order to investigate the role of the thiosemicarbazone moiety on activity, we also synthesized and tested compound **7**, the hydrazone analogue of **2**, the most active molecule in the thiosemicarbazone series.

To assess the role of metal chelation in their antiviral mode of action, we have selected **1** and **2** (**1** without activity and **2** with reasonable activity against the PA-Nter enzyme) and studied their interactions with Mg^{2+}, the ion

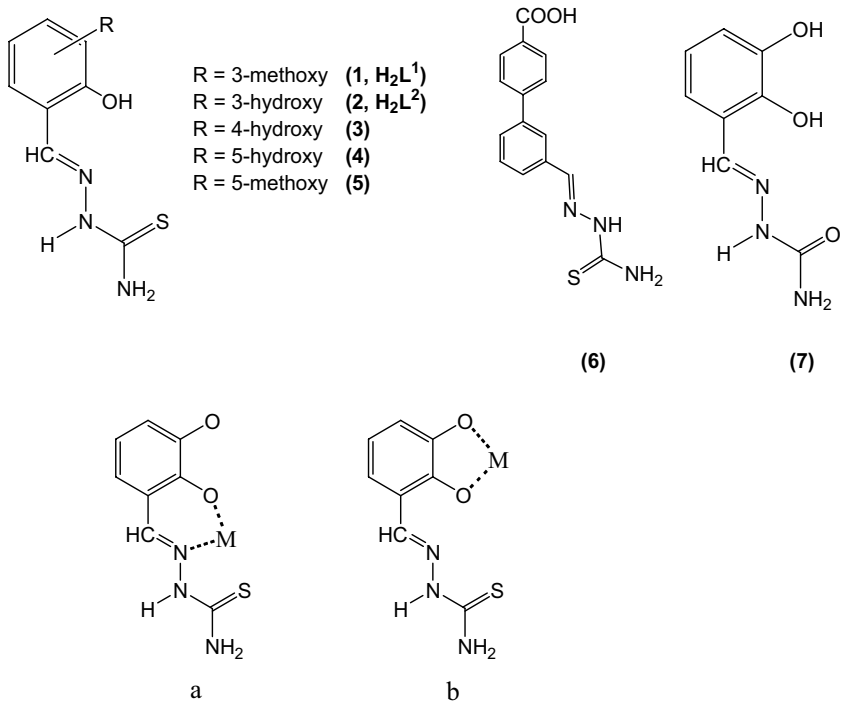

Fig. 3 Chemical structures of ligands **1**–**7** and the coordination modes **a** and **b** of **1**–**5**, involving the OH groups

that is probably involved in the endonuclease activity of the native influenza virus RdRp complex. The crystal structure of complex $Mg(HL^1)_2 2CH_3OH$ is also described (**1**, H_2L^1). Finally, docking studies on compounds **1** and **2** in complex with PA-Nter endonuclease were performed, to better elucidate the possible binding mode of these inhibitors.

Materials and methods

Chemistry

All reagents of commercial quality were used without further purification. Purity of compounds was determined by elemental analysis and verified to be ≥95 % for all synthesized molecules. NMR spectra were recorded at 25 °C on a Bruker Avance 400 FT spectrophotometer. The ATR-IR spectra were recorded by means of a Nicolet-Nexus (Thermo Fisher) spectrophotometer using a diamond crystal plate in the range of 4000–400 cm^{-1}. Elemental analyses were performed using a FlashEA 1112 series CHNS/O analyzer (Thermo Fisher) with gas-chromatographic separation. Electrospray mass spectral analyses (ESI–MS) were performed with an electrospray ionization (ESI) time-of-flight Micromass 4LCZ spectrometer. MS spectra were acquired in positive EI mode by means of a DEP-probe (Direct Exposure Probe) mounting on the tip a Re-filament with a DSQII Thermo Fisher apparatus, equipped with a single quadrupole analyzer.

Synthesis of the ligands

The TSCs **1**–**6** and the semicarbazone **7** were prepared following reported procedures [32]. Briefly, to a solution of the aldehyde in absolute ethanol, an equimolar amount of thiosemicarbazide was added, dissolved in the same solvent. In the synthesis of **7**, semicarbazide hydrochloride was used, which was suspended in ethanol and the pH adjusted to 7 using KOH 1 M. The mixture was refluxed for 6 h, cooled at room temperature and concentrated in vacuum. The resulting precipitate was filtered off, washed with cold ethanol and dried in vacuum.

*N-(2-Hydroxy-)-3-methoxybenzylidenethiosemicarbazide (**1**, H_2L^1)* Yield = 71 %. ^{1}H-NMR (DMSO-d_6, 25 °C), δ: 3.80 (*s*, 3H, OCH_3), 6.77 (t, 1H; J = 7.9 Hz, ArH), 6.96 (d, 1H, J = 7.8 Hz, ArH), 7.52 (d, 1H, J = 7.8 Hz, ArH), 7.87 (s, br, 1H, NH), 8.09 (s, br, 1H, NH), 8.40 (s, 1H; HC=N), 9.20 (s, br, 1H, OH), 11.39 (s, br, 1H; NH). ^{1}H-NMR (MeOD-d_4, 25 °C), δ: 3.90 (s, 3H, OCH_3), 6.84 (t, 1H; J = 7.9 Hz, ArH), 6.99 (d, 1H, J = 7.8 Hz, ArH), 7.43 (d, 1H, J = 7.8 Hz, ArH), 8.41 (s, 1H; HC=N). MS (EI, 70 eV), m/z (%) = 225.0 ($[M]^+$, 100); IR (cm^{-1}): ν_{NH} = 3459, 3339; ν_{OH} = 3158 (br); $\nu_{C=N}$ = 1596; $\nu_{C=S}$ = 1532, 821; ν_{OCH3} = 1258, 1056. Anal. Calcd. for $C_9H_{11}N_3O_2S{\cdot}0.5H_2O$: C 46.14; H 5.16; N 17.94. Found: C 45.92, H 4.82, N 18.24.

*N-(2,3-Dihydroxybenzylidene)-thiosemicarbazide (**2**, H_2L^2)* Yield = 75 %. ^{1}H-NMR (DMSO-d_6, 25 °C), δ: 6.63 (t, 1H;

J = 7.9 Hz, ArH), 6.79 (d, 1H, J = 7.8 Hz, ArH), 7.35 (d, 1H, J = 7.5 Hz, ArH), 7.86 (s, br, 1H, NH), 8.08 (s, br, 1H, NH), 8.36 (s, 1H; HC=N), 9.20 (s, vbr, 2H, OH), 11.37 (s, br, 1H; NH). ^{1}H-NMR (MeOD-d_4, 25 °C), δ: 6.75 (t, J = 7.9 Hz, 1H), 6.86 (dd, J = 7.9, 1.6 Hz, 1H), 7.14 (d, J = 7.9 Hz, 1H), 8.30 (s, 1H, HC=N). MS (EI, 70 eV), m/z (%) = 210.9 ([M]$^+$, 100); IR (cm^{-1}): ν_{NH} = 3364, 3256; ν_{OH} = 3173 (br); $\nu_{C=N}$ = 1620; $\nu_{C=S}$ = 1539, 825. Anal. Calcd. for $C_8H_9N_3O_2S{\cdot}0.5H_2O$: C 43.63; H 4.58; N 19.08. Found: C 43.33, H 4.48, N 18.98.

N-(2,4-Dihydroxybenzylidene)-thiosemicarbazide ***(3)*** Yield = 78 %. ^{1}H-NMR (DMSO-d_6, 25 °C), δ: 6.25–6.29 (m, 2H; ArH), 7.67 (d, 1H, J = 8.4 Hz, ArH), 7.74 (s, br, 1H, NH), 7.94 (s, br, 1H, NH), 8.24 (s, 1H; HC=N), 9.78 (s, br, 2H, OH), 11.17 (s, br, 1H; NH). MS (EI, 70 eV), m/z (%) = 211.0 ([M]$^+$, 100); IR (cm^{-1}): ν_{NH} = 3479, 3347; ν_{OH} = 3262, 3128 (br); $\nu_{C=N}$ = 1630; $\nu_{C=S}$ = 1582, 875. Anal. Calcd. for $C_8H_9N_3O_2S$ 1/3H_2O: C 44.23; H 4.48; N 19.34. Found: C 43.94, H 4.05, N 19.18.

N-(2,5-Dihydroxybenzylidene)-thiosemicarbazide ***(4)*** Yield = 85 %. ^{1}H-NMR (DMSO-d_6, 25 °C), δ: 6.68 (m, 2H; ArH), 7.22 (s, 1H, ArH), 7.78 (s, br, 1H, NH), 8.07 (s, br, 1H, NH), 8.30 (s, 1H; HC=N), 8.83 (s, br, 2H, OH), 9.21 (s, br, 2H, OH), 11.33 (s, br, 1H; NH). MS (EI, 70 eV), m/z (%) = 211.0 ([M]$^+$, 100); IR (cm^{-1}): ν_{NH} = 3427, 3328; ν_{OH} = 3048, 3002 (br); $\nu_{C=N}$ = 1623; $\nu_{C=S}$ = 1559, 942. Anal. Calcd. for $C_8H_9N_3O_2S$ 1/3H_2O: C 44.23; H 4.48; N 19.34. Found: C 44.11, H 4.39, N 19.18.

N-(2-Hydroxy-5-methoxybenzylidene)-thiosemicarbazide ***(5)*** Yield = 63 %. ^{1}H-NMR (DMSO-d_6, 25 °C), δ: 6.76–6.84 (m, 2H; ArH), 7.48 (s, 1H, ArH), 8.01 (s, br, 1H, NH), 8.13 (s, br, 1H, NH), 8.35 (s, 1H; HC=N), 9.44 (s, br, 2H, OH), 11.36 (s, br, 1H; NH). MS (EI, 70 eV), m/z (%) = 225.0 ([M]$^+$, 100); IR (cm^{-1}): ν_{NH} = 3412, 3304; ν_{OH} = 3120 (br); $\nu_{C=N}$ = 1626; $\nu_{C=S}$ = 1537, 821. Anal. Calcd. for $C_9H_{11}N_3O_2S$: C 47.99; H 4.92; N 18.65. Found: C 48.17, H 4.82, N 18.34.

N-(3-(1,1′-Biphenyl)-4-carboxylic acid)-thiosemicarbazide ***(6)*** Yield = 51 %. ^{1}H-NMR (DMSO-d_6, 25 °C), δ: 7.53 (t, J = 8 Hz, 1H; ArH), 7.78 (m, 2H, ArH), 7.89 (d, J = 8 Hz, 2H, ArH), 8.03 (d, 2H, ArH), 8.13–8.26 (m, 4H, ArH + HC=N + NH_2), 11.51 (s, br, 1H, NH), 13.00 (s, br, 1H, OH). MS (EI, 70 eV), m/z (%) = 298.9 ([M]$^+$, 60); IR (cm^{-1}): ν_{NH+OH} = 3432, 3263, 3143 (br); $\nu_{C=N}$ = 1606; ν_{NH2} = 1535. Anal. Calcd. for $C_{21}H_{16}N_2O_6S{\cdot}1.5H_2O$: C 55.21; H 4.94; N 12.88. Found: C 55.38, H 4.85, N 13.03.

N-(2,3-Dihydroxybenzylidene)-semicarbazide ***(7)*** Yield = 70 %. ^{1}H-NMR (DMSO-d_6, 25 °C), δ: 6.36 (s, br, 2H, NH_2), 6.64 (t, 1H; J = 7.9 Hz, ArH), 6.76 (d, 1H, J = 7.8 Hz, ArH), 7.17 (d, 1H, J = 7.5 Hz, ArH), 8.14 (s, 1H; HC=N), 9.21, 9.39 (s, br, 2H, OH), 10.17 (s, br, 1H; NH). ^{1}H-NMR (MeOD-d_4, 25 °C), δ: 6.75 (t, J = 7.9 Hz, 1H), 6.86 (dd, J = 7.9, 1.6 Hz, 1H), 7.14 (d, J = 7.9 Hz, 1H), 8.30 (s, 1H, HC=N). MS (EI, 70 eV), m/z (%) = 195.0 ([M]$^+$, 100); IR (cm^{-1}): ν_{NH} = 3455, 3350; ν_{OH} = 3166 (br); $\nu_{C=O}$ = 1694; $\nu_{C=N}$ = 1592. Anal. Calcd. for $C_8H_9N_3O_3$: C 49.23; H 4.65; N 21.53. Found: C 49.16, H 4.48, N 21.40.

$Mg(HL^1)_2$ 2.5H_2O ***(8)*** 0.5 mmol of H_2L^1 was dissolved in 20 ml of methanol and 4 eq. of NEt_3 was added. The solution turned yellow and it was stirred at r.t. for 30 min; 0.5 eq. of magnesium acetate was added and the reaction mixture was stirred at r.t. for 4 h, concentrated in vacuum and cooled overnight. The precipitate was filtered off and washed with water. Crystals suitable for X-ray diffraction analysis were obtained by slow evaporation of the mother liquors at room temperature. Yield: 74 %. ^{1}H-NMR (MeOD, 25 °C), δ: 3.89 (s, 3H, OCH_3); 6.84 (t, br, 1H, ArH), 6.98 (d, br, 1H, ArH), 7.42 (d, br, 1H, ArH), 8.40 (s, 1H, HC=N). MS–ESI, m/z (+, %) = 473 ([M + H]$^+$, 40); 495 ([M + Na]$^+$, 40). IR (cm^{-1}): ν_{NH} = 3334 (br); $\nu_{C=N}$ = 1596; $\nu_{C=S}$ = 1534; ν_{OCH3} = 1238, 1027. Anal. Calcd. for $C_{18}H_{20}N_6O_4Mg$ 2.5H_2O: C 41.75, H 4.87, N 16.23, S 12.38. Found: C 41.30, H 4.75, N 16.12, S 12.97.

$Mg(HL^2)_2$ ***(9)*** 0.5 mmol of H_2L^2 was dissolved in 20 ml of degassed methanol under nitrogen and 4 eq. of NEt_3 was added. The solution turned yellow and it was stirred at r.t. for 30 min; 0.5 eq. of magnesium acetate was added and the reaction mixture was stirred at r.t. for 4 h, concentrated in vacuum and cooled overnight. The precipitate was filtered off under inert atmosphere, washed with water and kept under nitrogen. Both the solution and the solid turn dark if exposed to air. ^{1}H-NMR (MeOD-d_4, 25 °C), δ: 6.47 (s, br, 2H), 6.81 (s, br, 1H), 8.12 (s, br, 1H, HC=N). MS–ESI, m/z (−, %) = 443 ([M]$^-$, 10); 210 ([HL^2]$^-$, 100). IR (cm^{-1}): ν_{NH+OH} = 3275, 3164 (br); $\nu_{C=N}$ = 1568; $\nu_{C=S}$ = 1534.

X-ray crystallography

Single crystals of **2** and of **$Mg(HL^1)_2{\cdot}2CH_3OH$** were selected and mounted on glass fibres to collect data on a SMART Breeze diffractometer. The crystals were kept at 293 K during data collection. Table 1 reports crystal data and structure analysis. Using Olex2 [33], the structure was solved with the SIR2004 [34] structure solution program using Direct Methods and refined with the ShelXL refinement package [35] using least squares minimisation. Anisotropic displacement parameters were refined for all non-hydrogen atoms. Hydrogen atoms were partly located on the Fourier difference map and partly introduced in

Table 1 Crystal data and structure refinement for **2** and **$Mg(HL^1)_2 \cdot 2CH_3OH$**

	$Mg(HL^1)_2 \cdot 2MeOH$	2
Empirical formula	$C_{20}H_{28}MgN_6O_6S_2$	$C_{10}H_{15}N_3O_3S$
Formula weight	536.91	257.31
Temperature/K	293(2)	293
Crystal system	Orthorhombic	Monoclinic
Space group	P2nn	$P2_1/c$
a/Å	7.878(1)	9.3259(6)
b/Å	10.639(2)	13.5879(9)
c/Å	31.921(5)	10.1652(6)
α/°	90	90
β/°	90	101.2117(9)
γ/°	90	90
Volume/Å^3	2675.4(7)	1263.5(1)
Z	4	4
ρ_{calc} g/cm^3	1.333	1.353
μ, mm^{-1}	0.267	0.257
F(000)	1128.0	544.0
Radiation	MoKα (λ = 0.71073)	MoKα (λ = 0.71073)
2Θ range for data collection/°	2.552–44.106	4.452–63.216
Reflections collected	21,724	19,770
Independent reflections	3296 [$R_{int} = 0.0818$, $R_{sigma} = 0.0481$]	4033 [$R_{int} = 0.0263$, $R_{sigma} = 0.0184$]
Data/restraints/parameters	3296/7/326	4033/0/174
Goodness-of-fit on F^2	1.073	1.031
Final *R* indexes [$I \geq 2\sigma(I)$]	$R_1 = 0.0702$, $wR_2 = 0.1916$	$R_1 = 0.0442$, $wR_2 = 0.1267$
Final *R* indexes [all data]	$R_1 = 0.0855$, $wR_2 = 0.2057$	$R_1 = 0.0492$, $wR_2 = 0.1311$
Largest Δ*F* max/min/e Å^{-3}	1.09/−0.38	0.81/−0.71
Flack parameter	0.43(7)	

calculated positions riding on their carrier atoms. Hydrogen bonds were analysed with PARST97 [36] and the Cambridge Structural Database software [37, 38] was used for the analysis of the crystal packing. Table 1 summarizes crystal data and structure determination results. Crystallographic data (excluding structure factors) for **2** and **$Mg(HL^1)_2 \cdot 2CH_3OH$** have been deposited with the Cambridge Crystallographic Data Centre as supplementary publication no. CCDC 1049845–1049846. Copies of the data can be obtained free of charge on application to CCDC, 12 Union Road, Cambridge CB2 1EZ, UK (fax: (+44) 1223-336-033; e-mail: deposit@ccdc.cam.ac.uk).

Biology

Production of recombinant influenza virus PA-Nter protein

The coding sequence for PA-Nter (i.e. residues 1–217 from the PA protein of influenza virus strain A/X-31) was cloned in the pET28a(+) plasmid (Merck KGaA, Darmstadt, Germany) with an N-terminal 6xHis-tag, and this bacterial expression plasmid was transformed into *E. coli* BL21-CodonPlus cells (Agilent Technologies, Santa Clara, CA). These bacteria were grown to an OD of 0.6, when IPTG was added at a final concentration of 1 mM to induce expression of recombinant protein for 5 h at 37 °C. The bacterial cells were ruptured using a French press and the protein was purified by 6xHis-Ni–NTA chromatography (Qiagen, Valencia, CA), followed by buffer exchange using PD-10 desalting columns (GE Healthcare, Diegem, Belgium) to keep the protein in storage buffer (50 mM Tris–HCl pH 8, 100 mM NaCl, 10 mM *β*-mercaptoethanol, 50 % glycerol). Protein purity was verified by SDS-PAGE with Coomassie Blue staining, and protein concentration was determined by Bradford assay. Finally, the purified protein was divided in aliquots and stored at −80 °C.

Plasmid-based endonuclease assay

The enzymatic PA-Nter assay was performed according to a published method [22] with minor modifications [20]. One microgram of recombinant PA-Nter was incubated

with 1 μg (16.7 nM) of single-stranded circular DNA plasmid M13mp18 (Bayou Biolabs, Metairie, Louisiana) in the presence of the test compounds and at a final volume of 25 μL. The assay buffer contained 50 mM Tris–HCl pH 8, 100 mM NaCl, 10 mM β-mercaptoethanol and 1 mM $MnCl_2$. The reaction was incubated at 37 °C for 2 h and then stopped by heat inactivation (80 °C, 20 min). The endonucleolytic digestion of the plasmid was visualized by gel electrophoresis on a 1 % agarose gel with ethidium bromide staining, and the amount of remaining intact plasmid was quantified by ImageQuant TL software (GE Healthcare).

The percentage inhibition of endonuclease activity was plotted against the compound concentration on a semi-logarithmic plot, using GraphPad Prism software (GraphPad Software, La Jolla, CA). Values were the mean ± S.E.M. of three independent experiments. The 50 % inhibitory concentrations (IC50) were obtained by nonlinear least squares regression analysis. The known PA-Nter inhibitor 2,4-dioxo-4-phenylbutanoic acid (DPBA) was included as the reference compound.

Cells and media

Madin–Darby canine kidney (MDCK) cells (a kind gift from M. Matrosovich, Marburg, Germany) and human embryonic kidney 293T (HEK293T) cells (purchased from Thermo Scientific) were grown in Dulbecco's modified Eagle medium (DMEM) supplemented with 10 % foetal calf serum (FCS), 1 mM sodium pyruvate and 0.075 % sodium bicarbonate. Virus experiments were performed in MDCK infection medium, consisting of Ultra MDCK medium (Lonza, Basel, Switzerland) supplemented with 0.0225 % sodium bicarbonate, 2 mM L-glutamine and 2 μg/mL tosyl phenylalanyl chloromethyl ketone (TPCK)-treated trypsin (Sigma-Aldrich). The cells were incubated in a 5 % CO_2 humidified atmosphere.

vRNP reconstitution assay

The assay to determine the inhibitory effect of the compounds on reconstituted influenza virus vRNPs is described in more detail elsewhere [39, 40]. Briefly, the four relevant expression plasmids derived from influenza A/PR/8/34 (i.e. pVP-PB1, pVP-PB2, pVP-NP and pVP-PA; generously donated by M. Kim [41], Korea Research Institute of Chemical Technology, Daejeon, South Korea) were combined with a firefly luciferase reporter plasmid (also a kind gift from M. Kim) and cotransfected into HEK293T cells using Lipofectamine 2000. After 24 h of incubation at 37 °C in the presence of the test compounds, luciferase activity was determined using the ONE-Glo luciferase assay system (Promega). The 50 % effective concentration (EC_{50}) was defined as the compound concentration causing 50 % reduction in the vRNP-driven firefly luciferase signal, as compared to cells receiving medium instead of compound. These EC_{50} values were calculated by interpolation assuming a semi-log dose–response effect. In parallel, the compound cytotoxicity, expressed as CC_{50} (50 % cytotoxic concentration) was determined using the spectrophotometric MTS cell viability assay (CellTiter 96 AQueous One Solution Cell Proliferation Assay; Promega). The CC_{50} values were defined as the compound concentration reducing cell viability in untransfected HEK293T cells by 50 %, as compared to the wells receiving medium instead of compound. Ribavirin was included as the reference compound.

Virus yield assay

To determine anti-influenza virus activity in cell culture, a virus yield assay was performed [40]. One day prior to infection, MDCK cells were seeded into 96-well plates at 25,000 cells per well. At day 0, the test compounds were added at serial dilutions, immediately followed by infection with influenza A/PR/8/34 virus. The multiplicity of infection (MOI) was 150 $CCID_{50}$ per well (50 % cell culture infectious dose; determined by the method of Reed and Muench [42]). After 24 h of incubation at 35 °C, the supernatants were harvested and stored at −80 °C. The viral copy number in these samples was estimated by a one-step quantitative real-time reverse transcription (qRT)-PCR assay (CellsDirect One-Step qRT-PCR kit; Invitrogen, Life Technologies, Gent, Belgium), with influenza virus M1-specific primers and probe (see [43] for all details). An M1-plasmid standard was included to allow absolute quantification. The EC_{99} and EC_{90} values were calculated by interpolation from data of at least three experiments and defined as the compound concentration causing, respectively, a 2-log10 and 1-log10 reduction in viral RNA (vRNA) copy number, as compared to the virus control receiving no compound. In parallel, uninfected MDCK cells were used to determine the CC_{50} values of the compounds after 24 h incubation, using the MTS cell viability assay (CellTiter 96 AQueous One Solution Cell Proliferation Assay; Promega). Ribavirin was included as the reference compound.

Computational studies

The crystal structure of PA endonuclease in complex with epigallocatechin-3-gallate was retrieved from the RCSB Protein Data Bank (entry code 4AWM). The ligand and water molecules were discarded and the hydrogens were added to protein by Discovery Studio 2. The epigallocatechin-3-gallate, L-742,001 and 2-(4-(1H-tetrazol-5-yl) phenyl)-5-hydroxypyrimidin-4(3H)-one structures were

extracted from their X-ray complexes, and the other structures of the ligands were constructed using Discovery Studio 2.5.5 (Accelrys, Discovery Studio) and energy minimized using the Smart Minimizer protocol (1000 steps) which combines the Steepest Descent and the Conjugate Gradient methods.

The ligands minimized in this way were docked in their corresponding proteins by means of Gold Suite 5.0.1 [44]. The region of interest used by Gold program was defined to contain the residues within 15 Å from the original position of the ligand in the X-ray structure. The side-chain of the residue Tyr24 was allowed to rotate according to the internal rotamer libraries in GOLD Suite 5.0.1. GoldScore was chosen as fitness function and the standard default setting was used in all calculations and the ligands were submitted to 100 genetic algorithm runs. The "allow early termination" command was deactivated. Results differing by less than 0.75 Å in ligand-all atom RMSD were clustered together. The best GOLD-calculated conformation was used both for analysis and representation.

Results and discussion

Chemistry

The ligands **1**–**6** (Fig. 3) were easily prepared in high yields by condensation of the thiosemicarbazide and the substituted benzaldehyde; they were characterized by spectroscopic tools, mass spectrometry and elemental analysis. **2** was also characterized by single crystal X-ray diffraction. In **6** the OH/OCH_3 groups are substituted by a carboxylic moiety, which retains good affinity for magnesium ions, following a suggestion emerged in the research for new inhibitors of HIV RNase H [45], which has two magnesium ions in its active site. In the IR spectra of **1**–**6** the C = S stretching absorptions are at about 1530–1580 and 820–940 cm^{-1}; in the ^{1}H-NMR spectra, the resonances of the iminic proton (about 8.0 ppm) and of the hydrazonic NH and of NH_2 (11.3 ppm and 7.8–8.0 ppm, approximately) are evident. Isomerism around the C=N bond is possible, but in the ^{1}H-NMR spectra registered in d_6-DMSO there is only one set of signals: evidently, all the ligands are in the *E* form in solution. Even if these ligands can give rise to a thione-thiol equilibrium, no evidence was obtained about the presence of the thiolic form in solution. Analogous considerations can be made for **7**, the hydrazonic analogue of compound **2**.

Ligands **1**–**5** are very versatile: they possess both soft and hard donor atoms and they can act as bidentate or tridentate chelating ligands. Complexes of salicylaldimine thiosemicarbazones with divalent metals like Pd(II), Zn(II), Cu(II), Ni(II) have been studied previously [46–51], but little is known about their interactions with magnesium ions [52]. Magnesium is a hard Lewis acid and so coordination of the sulphur atom could be excluded. It is known that salicylaldimine ligands can be NO-coordinated to magnesium (A, Fig. 3), but in **1** and **2**, with two oxygen donors in *ortho*, coordination B (Fig. 3) is also plausible. Since chelation of the divalent metal cofactors within the active site of the influenza virus PA endonuclease provides the possible basis for their antiviral activity [17], we decided to clarify the coordination properties of two of these ligands (**1** and **2**, H_2L^1 and H_2L^2, respectively) towards Mg^{2+}. The ligands were combined with magnesium acetate to react in the presence of triethylamine as a base to afford the corresponding metal complexes **8** and **9**. It is worth noting that, in the case of **2**, the reaction was executed under inert atmosphere, since the reaction mixture became dark when exposed to air. In order to verify the influence of the metal to ligand ratio or the pH, different reaction conditions were used with **1** (1:1 and 1:2 metal to ligand ratio; up to 4 equivalents of base), but only with a 1:2 metal to ligand ratio and in the presence of 4 equivalents of base, a metal complex was isolated.

The infrared spectrum of both **8** and **9** displays bands associated with the NH group (3163–3460 cm^{-1}), thus indicating that this functionality is not deprotonated. The bands associated with the C=S stretching are unaffected upon complexation; therefore, it can be assumed that this group is not involved in coordination, as confirmed by X-ray diffraction analysis on **8**. In the IR spectrum of **8** the stretching of the methoxy group is slightly shifted compared to the free ligand, suggesting a possible involvement in coordination. The ^{1}H-NMR spectrum of **8** registered in d_6-DMSO shows the presence of two sets of signals: one set corresponds to the free ligand, while the second one corresponds to the metal complex. The use of a coordinating solvent, therefore, causes the partial decoordination of the ligand. On the contrary, in the ^{1}H-NMR spectrum in MeOD, where the solubility is, however, low, there is a unique set of signals: the ligand coordinates to the metal in a bidentate fashion only when a poor coordinating solvent is present. The ^{1}H-NMR spectrum of **9** shows very broad signals, which might indicate that a fluxional behaviour can exist in solution. It is worth noting that complex **9** is not stable if exposed to air both in solution and at the solid state. Mass spectra confirmed the presence in solution of complexes of type $M(HL)_2$ and elemental analysis confirmed the proposed stoichiometry, $\mathbf{Mg(HL^1)_2{\cdot}2.5H_2O}$, for **8**.

X-ray crystallography

Ligand **2** was crystallized from ethanol as the solvate form $\mathbf{2{\cdot}CH_3CH_2OH}$ (Table 1). The molecular structure, shown in Fig. 4, is perfectly planar, and the thiosemicarbazone

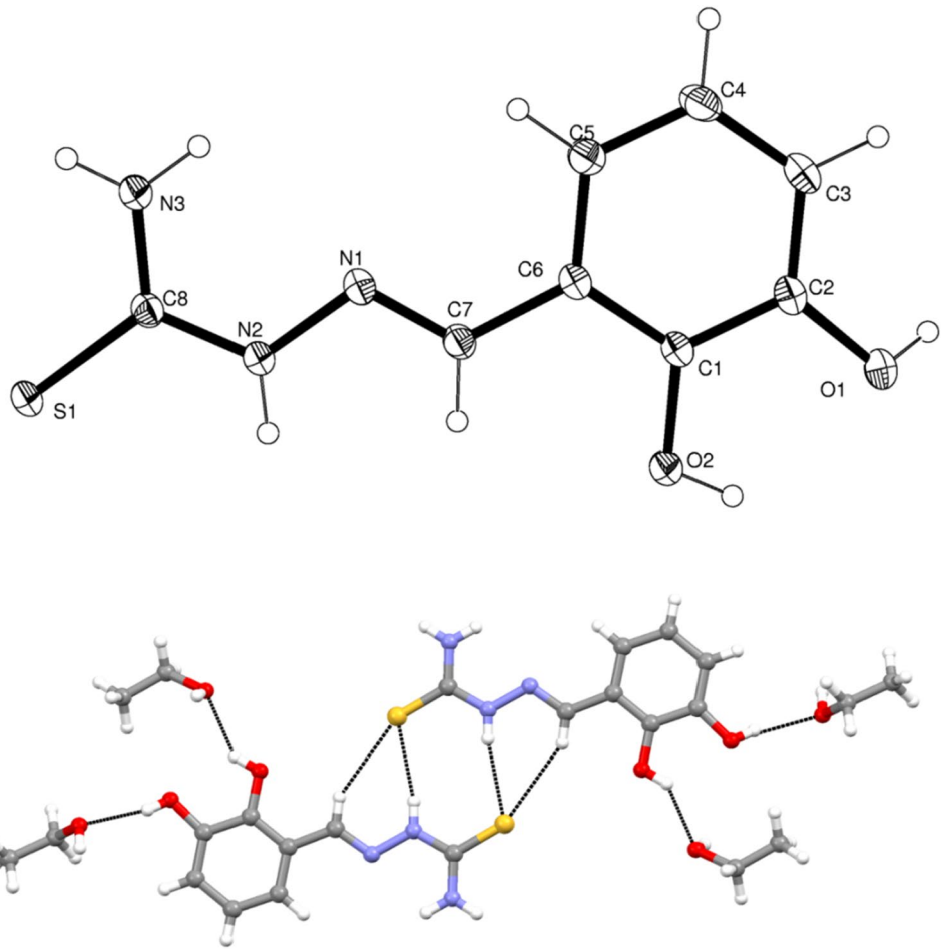

Fig. 4 Molecular structure and labelling of **2**, with thermal ellipsoids drawn at the 50 % probability level. *Bottom* supramolecular aggregation of **2** · **CH_3CH_2OH** in the solid, with dotted hydrogen bonds

chain is completely extended, with *trans* torsion angles larger than 175° along the chain. The *cis* configuration between the amide NH and the imidic CH favours the aggregation of coplanar molecular pairs by the interactions between these groups and the sulphur (Fig. 4, bottom) (N2–H…S1(i) = 3.401(1)Å, 167.2(1)°, C7–H…S1(i) = 3.762(1)Å, 152.0(1)°, i = 1 − *x*, −*y*, 2 − *z*). The dimeric assembly is surrounded by ethanol molecules linked by hydrogen bonds to the hydroxyl groups of **2** which act as donors: O2–H…O3(ii) = 2.816(2)Å, 141(2)°; O1-H…O3(iii) = 2.770(2)Å, 168(3)° (ii = 2 − *x*, *y* − 1/2, 3/2 − *z*; iii = 2 − *x*, −*y*, 1 − *z*). The ethanol molecule in turn donates a hydrogen bond to the sulphur atom (O3–H…S1(iv) = 3.218(1)Å, 158(2)°, iv = *x* + 1, *y*, *z*) while the $-NH_2$ moiety donates a hydrogen bond to one hydroxyl group (N3–H…O2(v) = 3.013(2)Å, 178(2)°, v = 1 − *x*, 1/2 + *y*, 3/2 − *z*), thus generating a three-dimensional hydrogen bond network.

Complex **$Mg(HL^1)_2 \cdot 2CH_3OH$** crystallizes from methanol in the orthorhombic P2nn space group (Table 1). The neutral complex comprises two monodeprotonated $(HL^1)^-$ ligands coordinated in a bidentate mode to the magnesium cation by means of the methoxy group and of the deprotonated hydroxyl group, forming two planar five-membered chelation rings; two *cis* methanol molecules complete the octahedral coordination (Fig. 5) and the overall complex molecule has a pseudo twofold rotation axis relating the two ligands and the two methanol molecules.

The *mer* configuration of the two bidentate ligand confers optical activity to the complex; the crystal is, however, racemic due to the presence of reflection planes. The thiosemicarbazone arms are protonated on the amidic nitrogen and are noticeably distorted due to intramolecular interactions. In fact the amide NH and the imidic CH groups are in *trans* configuration, and the latter is also turned away from the hydroxyl group, in contrast to the situation observed for the free ligand **2** (H_2L^2), whose molecular structure is comparable to **1** (H_2L^1). The torsion angles along the chains of the two ligands $(HL^1)^-$ in the complex differ significantly from the 0/180° value of the extended conformation of the free ligand, reported in parentheses: C1–C2–C8–N1 = 150/155°(−5°), C2–C8–N1–N2 = 7/3° (180°), C8–N1–N2–C9 = −166/−162°(175°), N1–N2–C9–N3 = 9/5°(−2°). These conformational distortions are mainly due to strong intramolecular hydrogen bonds between the amidic NH and the coordinated deprotonated

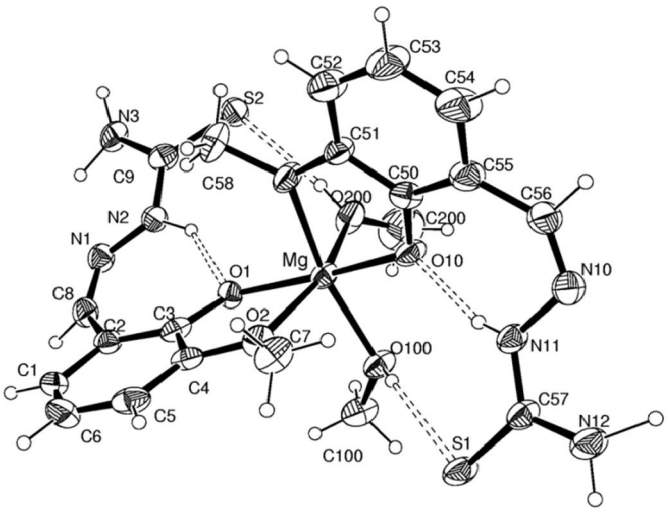

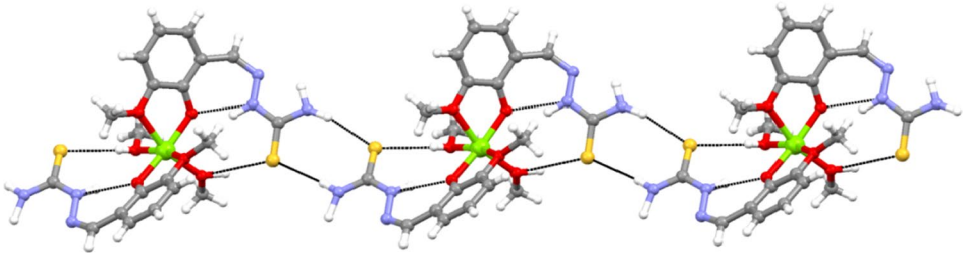

Fig. 5 Molecular structure and labelling of complex $\mathbf{Mg(HL^1)_2{\cdot}2CH_3OH}$, with thermal ellipsoids drawn at the 50 % probability level and dashed intramolecular hydrogen bonds. *Bottom* supramolecular aggregation of $\mathbf{Mg(HL^1)_2{\cdot}2CH_3OH}$ in the solid, with dotted hydrogen bonds

hydroxyl oxygens (N2–H…O1 = 2.582(1)Å, 147(1)°; N11–H…O10 = 2.589(1)Å, 153(1)°), and between the coordinated methanol molecules and the sulphur atoms (O100–H…S1 = 3.189(1)Å, 155(1)°; O200–H…S2 = 3.212(1)Å, 159(1)°). The $–NH_2$ moiety is involved in an intermolecular hydrogen bond to the sulphur atom generating an R22(8) ring (Fig. 5, bottom) which expands in ribbons along the diagonal *ab* (N3–H…S1(vi) = 3.410(1) Å, 162(1)°; N12–H…S2(vii) = 3.503(2)Å, 166(1)°, vi = $x + 1, y - 1, z$, vii = $x - 1, y + 1, z$). In both the free ligand and the complex the sulphur atoms are significantly involved in intermolecular interactions where they act as acceptors from –OH and –NH groups.

Biological activity

Compounds **1**–**6** were evaluated for their ability to inhibit endonuclease activity in an enzymatic assay with recombinant PA-Nter, and the results are presented in Table 2. Besides, their anti-influenza virus activity was determined in cell culture, in a virus yield assay in MDCK cells and in a vRNP reconstitution assay in HEK293T cells. We also evaluated the inhibitory activity of **1**–**6** against a broad panel of DNA [i.e. herpes simplex virus type 1, vaccinia virus and adenovirus, evaluated in infected human embryonic lung fibroblast (HEL) cells] and RNA viruses (Coxsackie B4 virus and respiratory syncytium virus, tested in HeLa cells; parainfluenza-3 virus and Punta Toro virus, tested in Vero cells). However, they were found to be inactive against these diverse viruses, with the exception of a modest activity of **2** against herpes simplex virus-1 (EC_{50} = 58 μM) and vaccinia virus (EC_{50} = 45 μM).

As can be seen in Table 2, compounds **2** and **4** displayed moderate activity in the PA-Nter enzymatic assay, with the catechol derivative **2** presenting the best result (IC_{50}: 37 μM). It is interesting to note that this compound has an activity profile similar to that of a 2,3-dihydroxyphenyl amide inhibitor that we recently reported [22], indicating the importance of the catechol pharmacophore for inhibition of the PA-Nter enzyme. In line with the enzymatic data on series **1**–**6**, compounds **2** and **4** were also the only derivatives showing antiviral activity in both cell culture assays. Compound **2** displayed an $EC_{99} \geq 87$ μM and $EC_{90} \geq 56$ μM in the virus yield assay, and an EC_{50} value of 63 μM in the vRNP reconstitution assay. For **4**, the corresponding values were 48, 34 and 22 μM, respectively. Additionally, compound **5** displayed weak inhibitory activity in the vRNP reconstitution assay, with an average IC_{50} value of 150 μM.

Even if the set of data is quite limited, some preliminary conclusions can be drawn. **1** and **2** can coordinate the divalent magnesium ion in the B mode, using the methoxy and OH groups (**1**) or two OH groups (**2**); however, **1** is inactive, while **2** has moderate activity. The same type of

Table 2 Inhibitory activity of compounds **1**–**7** in the enzymatic assay with influenza virus PA-Nter endonuclease, or cellular influenza virus assays based on virus yield or vRNP reconstitution

Compound	Enzyme assay with PA-Nter[a]	Virus yield assay in influenza virus-infected MDCK cells[b]				vRNP reconstitution assay in HEK293T cells[c]	
	IC_{50}	Antiviral activity		Cytotoxicity		Activity	Cytotoxicity
		EC_{99}	EC_{90}	MCC	CC_{50}	EC_{50}	CC_{50}
(1)	>500	>200	>200	≥200	>200	>200	>200
(2)	37	≥87	≥56	≥100	≥138	63	>200
(3)	>500	>200	>200	>200	>200	>200	>200
(4)	341	48	34	≥100	146	22	>200
(5)	>500	>200	>200	≥200	>200	150	>200
(6)	>500	>100	>100	>200	>200	>100	>200
(7)	24	ND	ND	ND	ND	107	>200
DPBA[d]	5.5	ND	ND	ND	ND	ND	ND
Ribavirin	ND	13	8.5	≥200	>200	9.3	>200

ND not determined

[a] Recombinant PA-Nter was incubated with the ssDNA plasmid substrate, a Mn^{2+}-containing buffer and test compounds. Cleavage of the substrate was assessed after 2 h incubation. The IC_{50} represents the compound concentration (in μM) to obtain 50 % inhibition of cleavage

[b] MDCK (Madin–Darby canine kidney) cells were infected with influenza A virus (strain A/PR/8/34) and incubated with the compounds for 24 h. The virus yield in the supernatant was assessed by real-time qPCR. The EC_{99} and EC_{90} values represent the compound concentrations (in μM) producing a 2-$\log_{10}$ or 1-$\log_{10}$ reduction in virus titer, respectively. The cytotoxicity, assessed in uninfected MDCK cells, was expressed as the CC_{50} value (50 % cytotoxic concentration, determined with the MTS cell viability assay, in μM)

[c] HEK293T (human embryonic kidney 293T) cells were cotransfected with the four vRNP-reconstituting plasmids and the luciferase reporter plasmid in the presence of the test compounds. The EC_{50} value represents the compound concentration (in μM) producing 50 % reduction in vRNP-driven firefly reporter signal, estimated at 24 h after transfection. The CC_{50} (in μM), i.e. the 50 % cytotoxic concentration, was determined in untransfected HEK293T cells by MTS cell viability assay

[d] DPBA, 2,4-dioxo-4-phenylbutanoic acid

substitution, i.e. moving from **4** (5-OH) to **5** (5-methoxy), has the same effect on biological activity [i.e. **4** is moderately active; **5** has very weak activity (vRNP reconstitution assay) or is inactive (virus yield assay)]. It is difficult to correlate this effect to a different coordinating ability of the ligands, in particular looking at **4** and **5**, which can both use mode A (Fig. 3). Similarly, a different coordination behaviour cannot explain the different activity of **3** and **4**. On the other hand, the finding that **4** has lower activity in the enzymatic assay than **2** could well be related to their different coordination mode to the magnesium ion in the active site of the PA-Nter enzyme.

To further investigate the role of the thiosemicarbazone moiety on activity, we evaluated the biological activity of compound **7**, the hydrazonic analogue of **2**. Compound **7** has three oxygens in the right orientation to chelate simultaneously two metal ions. It is worth noting that the replacement of the sulphur atom of **2** with an oxygen in compound **7** results in a slight improvement in the inhibitory activity against the PA-Nter enzyme, with the IC_{50} changing from 37 to 24 μM. This can be related to the improved ability of the ligand to interact with the metal cofactors, when a harder donor atom is present. However, the activity of **7** in the cellular vRNP assay is lower than that of the parent thiosemicarbazone **2,** thus suggesting that for the thiosemicarbazone compounds inhibition of PA-Nter endonuclease is not the only mode of action. In influenza virus-infected cells, in fact, the antiviral activity is higher for compound **4** than for **2**, and the other TSCs are inactive. Note that, in cell culture (i.e. in the virus yield and vRNP reconstitution assay), **4** produces antiviral activity at concentrations below 50 μM, while in the enzymatic assay its IC_{50} value was 341 μM. This suggests that the suppressive effect of **4** on influenza virus replication may not merely be related to direct inhibition of the endonuclease enzyme, since the compound may also affect other steps in the virus replicative cycle. These considerations are in line with our recent studies [20] showing the complex biological properties of some molecules proposed as metal chelating inhibitors of the influenza virus PA endonuclease.

Computational studies

In order to explain the difference of activity between compound **1** and **2,** docking simulations by Gold program [44] were performed using the structural coordinates (pdb code 4AWM) for the PA endonuclease in complex with epigallocatechin-3-gallate [14].

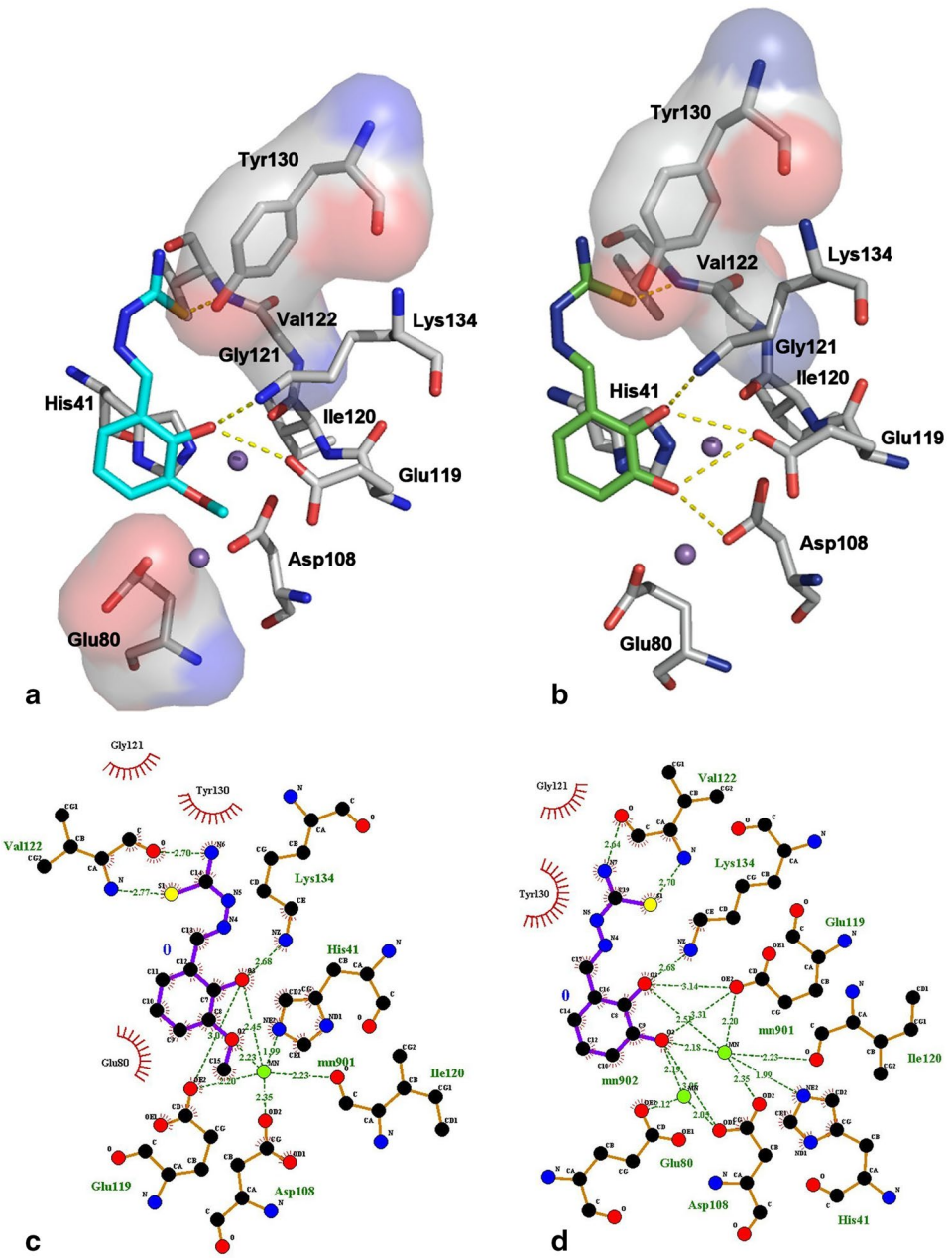

Fig. 6 Docking studies of PA endonuclease with compounds **1** (*cyan* **a**) and **2** (*green* **b**), respectively. Key residues of the pocket are presented using PyMOL [http://www.pymol.org]. Hydrogen bonds are illustrated by *dotted lines* while the divalent metal ions are shown as *purple spheres*. Schematic drawing of types of interactions of the compounds **1** (**c**) and **2** (**d**) generated using Ligplot [53]. *Dashed lines* are hydrogen bonds and *eyelashes* show residues involved in hydrophobic interactions

Considering that the side-chains of some residues change depending on which pocket the ligand is occupying, we superimposed some X-ray structures of complexes between PA endonuclease and known active ligands. We observed that the side-chain of the aminoacid Tyr24 showed a greater movement than the other residues and for this reason we considered it as a flexible residue during the docking procedure.

First, test docking calculations, using epigallocatechin-3-gallate, L-742,001 and 2-(4-(1H-tetrazol-5-yl)phenyl)-5-hydroxypyrimidin-4(3H)-one (Fig. 1) were carried out to compare experimental and predicted binding modes and to validate our docking protocol. Their best docking poses agreed well with the experimental binding modes with rmsd of 0.8, 1.2 and 0.7, respectively.

Later, compounds **1** and **2** were docked and the best docking poses were selected and analysed by Ligplot [53] revealing a similar binding mode (Fig. 6a, b).

The thiosemicarbazone portions of **1** and **2** share a very similar network of interactions with the residues into the active site (hydrophobic interactions with Gly121 and Tyr130 and hydrogen bonds with Val122). The salicylaldehyde portion is able to chelate one magnesium ion in the same way (B mode) for both derivatives, but the 3-hydroxy (**2**) and 3-methoxy (**1**) groups play different roles, engaging different interactions both with the second magnesium ion

and with some important aminoacidic residues. In particular, LigPlot analysis displays that the 3-OH of **2** forms an additional contact with the second metal ion and hydrogen bonds with the catalytic residues Asp108 and Glu119, stabilizing the molecule in the active site: these interactions, therefore, could explain the difference of activity between the two compounds.

Conclusions

We have started a project focused on the synthesis and biological evaluation of chemical scaffolds that are able to bind one or two metal ions in the PA-Nter active site and, in this way, can inhibit influenza virus replication [20, 22, 40]. From this perspective, salicylaldehyde thiosemicarbazones seem promising, because of their well-known coordinating abilities and biological properties. In the first evaluation reported here, positions 3, 4 and 5 of the phenyl ring were substituted with OH and OCH_3 donor groups to derive a structure–activity relationship. Compounds **2** and **4** displayed moderate activity in the PA Nter enzymatic assay and antiviral activity in both cell culture assays used in this study. In particular, compound **2**, with two OH groups in position 2 and 3 on the phenyl ring, is the most active and this is in line with the results recently reported by us with a 2,3-dihydroxyphenyl amide inhibitor [22] and the literature regarding the use of natural polyphenols for inhibiting influenza virus infection [54]. Thiosemicarbazones **1**–**5** are effectively able to coordinate magnesium(II) ion, as definitely proved by the structure of $\mathbf{Mg(HL^1)_2{\cdot}2CH_3OH}$, but it seems difficult to correlate their activity exclusively to this ability. For example, compound **5** is inactive, while **4** is moderately active, but structural differences between them (5-methoxy group in **5** instead of 5-OH group as in **4**) do not imply differences in chelating properties. The different activity could depend not only on a different mechanism of action, but also on the effect that Cohen sharply describes as "malleable interaction" in metal coordination by metalloenzyme inhibitors [55], to describe the large number of factors (donor atom identity, orientation, electrostatics, van der Waals interactions,…) that are involved in the inhibition mechanism. The semicarbazone **7**, that has three oxygen atoms and can coordinate simultaneously two metal ions in the enzyme active site, is more active than the corresponding thiosemicarbazone **2**. Following this suggestion, we are now working on polyhydroxylated acylhydrazones to exploit their potential as antiviral inhibitors [56].

Another point that deserves closer examination is the difference between the data obtained for **2** and **4** using different assays: in the enzyme assay, **2** is more active than **4**, but the opposite was seen in virus-infected cells and the vRNP reconstitution assay. Compound **4** probably acts by different antiviral mechanisms, not only metal chelation. This underscores that characterization of the activity of a new compound is possible only if different complementary assays are used.

Acknowledgments The authors thank the "Centro Interfacoltà Misure Giuseppe Casnati" of the University of Parma for facilities. L. Naesens and A. Stevaert acknowledge financial support from the Geconcerteerde Onderzoeksacties—KU Leuven (GOA/15/019/TBA) and the technical assistance from Wim van Dam, Leentje Persoons en Ria Van Berwaer.

References

1. Deyde VM, Xu X, Bright RA, Shaw M, Smith CB, Zhang Y, Shu Y, Gubareva LV, Cox NJ, Klimov AI (2007) J Infect Dis 196:249–257
2. Moscona A (2009) N Engl J Med 360:953–956
3. Memoli MJ, Davis AS, Proudfoot K, Chertow DS, Hrabal RJ, Bristol T, Taubenberger JK (2011) J Infect Dis 203:348–357
4. Van der Vries E, Schutten M, Fraaij P, Boucher C, Osterhaus A (2013) Adv Pharmacol 67:217–246
5. Vanderlinden E, Naesens L (2014) Med Res Rev 34:301–339
6. Honda A, Ishihama A (1997) Biol. Chem 378:483–488
7. Honda A, Mizumoto K, Ishihama A (2002) Proc Natl Acad Sci USA 99:13166–13171
8. Das K, Aramini JM, Ma LC, Krug RM, Arnold E (2010) Nat Struct Mol Biol 17:530–538
9. Dias A, Bouvier D, Crépin T, McCarthy AA, Hart DJ, Baudin F, Cusack S, Ruigrok RW (2009) Nature 458:914–918
10. Yuan P, Bartlam M, Lou Z, Chen S, Zhou J, He X, Lv Z, Ge R, Li X, Deng T, Fodor E, Rao Z, Liu Y (2009) Nature 458:909–913
11. Plotch SJ, Bouloy M, Ulmanen I, Krug RM (1981) Cell 23:847–858
12. Zhao C, Lou Z, Guo Y, Ma M, Chen Y, Liang S, Zhang L, Chen S, Li X, Liu Y, Bartlam M, Rao Z (2009) J Virol 83:9024–9030
13. DuBois RM, Slavish PJ, Baughman BM, Yun MK, Bao J, Webby RJ, Webb TR, White SW (2012) PLoS Pathog 8:e1002830
14. Kowalinski E, Zubieta C, Wolkerstorfer A, Szolar OH, Ruigrok RW, Cusack S (2012) PLoS Pathog 8:e1002831
15. Doan L, Handa B, Roberts NA, Klumpp K (1999) Biochemistry 38:5612–5629
16. Xiao S, Klein ML, LeBard DN, Levine BG, Liang H, MacDermaid CM, Alfonso-Prieto M (2014) J Phys Chem B 118:873–889
17. Rogolino D, Carcelli M, Sechi M, Neamati N (2012) Coord Chem Rev 256:3063–3086
18. Tomassini JE, Selnick H, Davies ME, Armstrong ME, Baldwin J, Bourgeois M, Hastings J, Hazuda D, Lewis J, McClements W, Ponticello G, Radzilowski E, Smith G, Tebben A, Wolfe A (1994) Antimicrob Agents Chemother 38:2827–2837
19. Hastings JC, Selnick H, Wolanski B, Tomassini JE (1996) Antimicrob Agents Chemother 40:1304–1307
20. Stevaert A, Nurra S, Pala N, Carcelli M, Rogolino D, Shepard C, Domaoal RA, Kim B, Alfonso-Prieto M, Marras SAE, Sechi M, Naesens L (2015) Mol Pharmacol 87:323–337
21. Singh SB (1995) Tetrahedron Lett 36:2009–2012
22. Carcelli M, Rogolino D, Bacchi A, Rispoli G, Fisicaro E, Compari C, Sechi M, Stevaert A, Naesens L (2014) Mol Pharm 11:304–316
23. Parkes KEB, Ermert P, Fässler J, Ives J, Martin JA, Merrett JH, Obrecht D, Williams G, Klumpp K (2003) J Med Chem 46:1153–1164

24. Sagong HY, Parhi A, Bauman JD, Patel D, Vijayan RS, Das K, Arnold E, LaVoie EJ (2013) ACS Med Chem Lett 4:547–550
25. Knox JJ, Hotte SJ, Kollmannsberger C, Winquist E, Fisher B, Eisenhauer EA (2007) Invest New Drugs 25:471–477
26. Kang IJ, Wang LW, Hsu TA, Yueh A, Lee CC, Lee YC, Lee CY, Chao YS, Shih SR, Chern JH (2011) Bioorg Med Chem Lett 21:1948–1952
27. Quenelle DC, Keith KA, Kern ER (2006) Antiv Res 71:24–30
28. Debebe Z, Ammosova T, Breuer D, Lovejoy DB, Kalinowski DS, Kumar K, Jerebtsova M, Ray P, Kashanchi F, Gordeuk VR, Richardson DR, Nekhai S (2011) Mol Pharmacol 79:185–196
29. Pelosi G, Bisceglie F, Bignami F, Ronzi P, Schiavone P, Re MC, Casoli C, Pilotti E (2010) J Med Chem 53:8765–8769
30. Torti SV, Torti FM (2013) Nat Rev Cancer 13:342–355
31. Pelosi G (2010) Open Crystallogr J 3:16–28
32. Sacconi L (1954) Z Anorg Allg Chem 275:249–256
33. Dolomanov OV, Bourhis LJ, Gildea RJ, Howard JAK, Puschmann H (2009) J Appl Cryst 42:339–341
34. Burla MC, Caliandro R, Camalli M, Carrozzini B, Cascarano GL, De Caro L, Giacovazzo C, Polidori G, Siliqi D, Spagna R (2007) J Appl Cryst 40:609–613
35. Sheldrick GM (2008) Acta Cryst A64:112–122
36. Nardelli M (1995) J Appl Cryst 28:659
37. Allen FH, Kennard O, Taylor R (1983) Acc Chem Res 16:146–153
38. Bruno IJ, Cole JC, Edgington PR, Kessler M, Macrae CF, McCabe P, Pearson J, Taylor R (2002) Acta Crystallogr B 58:389–397
39. Meneghesso S, Vanderlinden E, Stevaert A, McGuigan C, Balzarini J, Naesens L (2012) Antiviral Res 94:35–43
40. Stevaert A, Dallocchio R, Dessì R, Pala N, Rogolino D, Sechi M, Naesens L (2013) J Virol 87:10524–10538
41. Kim M, Kim SY, Lee HW, Shin JS, Kim P, Jung YS, Jeong HS, Hyun JK, Lee CK (2013) Antiviral Res 100:460–472
42. Reed LJ, Muench H (1938) Am J Epidemiol 27:493–497
43. Vanderlinden E, Göktas F, Cesur Z, Froeyen M, Reed ML, Russell CJ, Cesur N, Naesens L (2010) J Virol 84:4277–4288
44. Jones G, Willett P, Glen RC, Leach AR, Taylor R (1997) J Mol Biol 267:727
45. Gong Q, Menon L, Ilina T, Miller LG, Ahn J, Parniak MA, Ishima R (2011) Chem Biol Drug Des 77:39–47
46. Enyedy ÉA, Zsigó É, Nagy NV, Kowol CR, Roller A, Keppler BK, Kiss T (2012) Eur J Inorg Chem 2012(25):4036–4047
47. Lobana TS, Kumari P, Hundal G, Butcher RJ (2010) Polyhedron 29:1130–1136
48. Chellan P, Stringer T, Shokar A, Dornbush PJ, Vazquez-Anaya G, Land KM, Chibale K, Smith GS (2011) J Inorg Biochem 105:1562–1568
49. Ramachandran E, Kalaivani P, Prabhakaran R, Rath NP, Brinda S, Poornima P, Padma VV, Natarajan K (2012) Metallomics 4:218–227
50. Kalaivani P, Prabhakaran R, Dallemer F, Poornima P, Vaishnavi E, Ramachandran E, Padma VV, Renganathan R, Natarajan K (2012) Metallomics 4:101–113
51. West DX, Salberg MM, Bain GA, Liberta AE, Valdés-Martínez J, Hernández Ortega S (1996) Transit Met. Chem. 21:206–212
52. Sahadev RKS, Sindhwani SK (1992) Thermochim Acta 202:291–299
53. Laskowski RA, Swindells MB (2011) J Chem Inf Mod 51:2778
54. Yang ZF, Bai LP, Huang WB, Li XZ, Zhao SS, Zhong NS, Jiang ZH (2014) Fitoterapia 93:47–53
55. Martin DP, Blachly PG, McCammon JA, Cohen SM (2014) J Med Chem 57:7126–7135
56. Rogolino D, Carcelli M, Bacchi A, Compari C, Contardi L, Fisicaro E, Gatti A, Sechi M, Stevaert A, Naesens L (2015) J Inorg Biochem 150:9–17